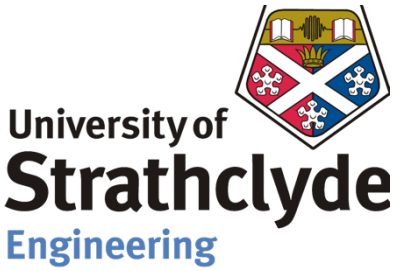

Department of Mechanical and Aerospace Engineering

Modelling and Design of a Wind Turbine Blade for Structural Integrity Analysis

Author: Jack Corkery

Supervisor: Dr. Haofeng Chen

A thesis submitted in partial fulfilment for the requirement of degree in

Master of Science in Sustainable Engineering: Renewable Energy Systems and the Environment

2021

Copyright Declaration

Signed: Jack Corkery Date: 17th August 2021

Abstract

The aim of this study was to further develop data on the structural integrity of wind turbine blades by designing and modelling a wind turbine blade based upon current wind turbine blade specifications and undergoing a fatigue analysis. The model uses available geometrical data from the NREL 5MW turbine and the Vestas 117 4.2MW turbine in order to approximate a large scale, upwind, horizontal, axis triple bladed wind turbine. The model uses fibre glass-epoxy composite as a material property. CFD and FEM calculations were achieved in order to analyse its structural integrity. For a rotor radius of 58.5m, the blade deformation was found at a maximum of 1.8874m at a maximum operational wind-speed of 23m/s. A modal analysis was carried out and the natural frequency of the blade was found to be 1.0236Hz. Finally, a fatigue analysis was carried out at the maximum operational wind speed where it was found that the number of load cycles before failure, $N \approx 100{,}000{,}000$ for the fibre glass-epoxy composite wind turbine blade. More continued work is to be done to carry out a mesh refinement analysis and to study a wider variety of parameters.

Acknowledgements

I would like to formally express my gratitude to my supervisor, Dr. Haofeng Chen for guiding this masters level project and introducing me to this new topic of structural integrity engineering.

I would like to thank my parents, Pat Corkery and Margaret Corkery who have supported and inspired my academic career.

Finally, I would like to give a special thanks to my house mate, Dylan O Mahony for always being there when I needed him.

Table of Contents

List of Figures

List of Tables

Nomenclature

Symbol	Description	Units
A	Area	m^2
C_D	Drag coefficient	-
C_L	Lift coefficient	-
C_P	Power coefficient	-
C_T	Torque coefficient	-
C	Chord length	m
E_k	Kinetic energy	J
E	Young's modulus	Pa
F	Force	N
f	Camber position	m
G	Shear modulus	Pa
h	Tower height	m
m	Mass	kg
N	Cycles to failure	-
P	Power	W
p	Momentum	kgm/s
P_T	Power output of turbine	W
R_D	Drag force	N
R_L	Lift force	N
r	Radius	m
S_1	First principal stress	Pa
S_2	Middle principal stress	Pa
S_3	Third principal stress	Pa
S_u	Ultimate stress	Pa
S_{vm}	Von Mises stress	Pa
T	Torque	Nm

T_R	Torque of turbine	Nm
V	Velocity	m/s
x_f	Maximum camber	m
α	Angle of attack	°
ε	Strain	-
λ	Tip speed ratio	-
ρ	Density	Kg/m^3
σ	Stress	Pa
σ_a	Stress amplitude	Pa
σ_{eqv}	Modified stress amplitude	Pa
τ_r	Viscosity	Kg/m·s
ω	Angular velocity	s^{-1}
υ	Poisson's ratio	-

1.0 Introduction

We are currently living through a time where scientists and engineers alike are all racing climate change in the hope to possibly halt its effects and prevent global disaster. Investors are bidding their money on clean, renewable energy as the most effective method of doing so, by reducing the demand for fossil fuels. Amongst these clean, renewable energies, the wind energy industry in particular has exploded in the 21st century. According to some analysts, this was due to a surge in the number of people concerned about climate change. [1] Wind power has since become the fastest growing energy technology in the world. [2] Global onshore wind energy potential is estimated to be approximately 119.5 petawatt hours per year, allowing for much further growth of the industry. [3] This provides an excellent opportunity to expand on the wind energy industry and implement this growth. Whilst doing so, it is just as important to continue building upon the knowledge of wind turbines. This allows us to harness wind energy potential as efficiently and as cleanly as possible.

1.1 Wind turbine challenges

Amongst the wind industry it is a commonly known problem that wind turbines require a great deal of maintenance to keep them running in a safe and efficient manner. Blade failures in particular exhibit one of the biggest numbers of structural incidents recorded. [4] This may include total blade failures or breaks in the blade. Blade failure is a result of cracks in the blade which arise from fatigue or material defects. [5, 6], Even minor blade damages may cause unbalance in the rotating body which induces extra stress, speeding up the degradation process of the wind turbine. [7] Lightning strikes and ice build-up are also commonly known causes of blade failures. [8] A much wider scope of problems may incur in further areas of the wind turbine such as the power system, the auxiliary system or fatigue in other structures such as the tower or the hub.

Blade damage requires extensive repair with a long down time. Down time leads to a total reduction in renewable energy generation from a wind farm and thus a reduction in revenue for the wind farm. Furthermore, the cost of the blades accounts for 15–20% of the total turbine cost. [9] In addition, the replacement of wind turbine blades is not environmentally friendly, not only due to the down time in renewable energy generation but due to the manufacturing process of a wind turbine blade. Information provided by wind blade

manufacturers shows that each blade can weigh as much as 12 tonnes and that the manufacturing process generates around 10–15% of waste. [10] In addition, 76.2% of waste produced in the manufacturing process is inorganic material. [11]

1.2 Goals of this project

The goal of this project is to design a wind turbine blade based off current modern blade technologies and analyse its structural integrity, specifically to conduct a fatigue assessment analysis. Designing the wind turbine blade consists of using a computer aided design (CAD) with limited wind turbine rotor specifications to model the more detailed geometry. Analysing the structural integrity of the wind turbine blade will consist of carrying out a fluid flow analysis, a static structural analysis, and a modal analysis. Decisions for the model must be carefully considered, such as whether it is a partial or complete assembly, or if it includes solid and or surface bodies. Approximations and boundary conditions must be carefully determined. The material properties must also be assigned to various parts of the geometry and finally, realistic loads were assigned to the simulation.

Thus, by the end of this experiment, one will have developed a methodology for designing and studying a modern wind turbine blade in order to carry out a structural integrity analysis to determine the structural performance and the number of cycles to failure. By carrying out a structural integrity analysis one can make informed design decisions based on the turbine blade longevity.

2.0 Theory and background

2.1 Wind turbine fundamentals

The fundamental role of a wind turbine is to convert kinetic energy contained in an air stream into electrical power. This is done in via a turbine rotor/blade where the kinetic energy is first converted into mechanical work. The rotor is then attached to a generator through a gearbox where the mechanical work is converted into electrical power.

2.1.1 Classifications

Some wind turbine sites can contain over one hundred active wind turbines. These can be either onshore or offshore wind farms. Offshore wind turbine farms tend to be faster growing due to the larger area of space available and less planning restrictions. Offshore wind turbines also have the benefit of being in open areas which allow for higher and more consistent wind speeds. [12] This means they experience less turbulence and as a result are less prone to fatigue damage. Maintenance and construction for offshore wind farms may be more expensive and this is the benefit of onshore wind farms. They are also easier to connect to the national electricity grid with less losses through cables.

Modern wind turbines can be classified depending on the rotational axis of the wind turbine blades. Horizontal axis wind turbines (HAWTs) are far more common as they have a low cut-in wind speed. Since they can be turned at an angle to the direction of incoming wind, they exhibit easy furling. Vertical axis wind turbines (VAWTs) are a much older design of wind turbine, generally with a lower energy efficiency. Another major problem of VAWTs is faster fatigue damage on the blades as a result of the cyclic aerodynamic stress. [13] Although VAWTs are much less common they benefit by being much cheaper to construct since the gearbox and generator can be situated on ground level. This is shown in figure 1 as a side by side comparison.

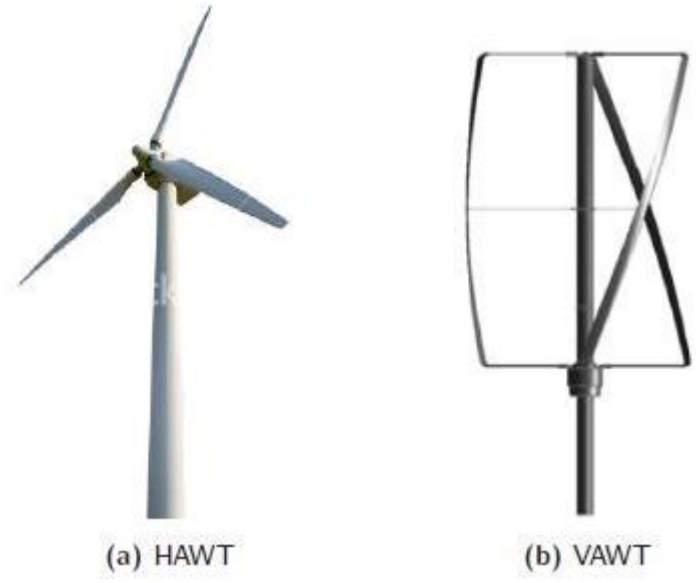

Figure 1: Comparison between HAWTs and VAWTs [14]

HAWTs may be further classified by the number of wind turbine blades attached to the hub. They could be single bladed, two bladed, three bladed or multi bladed. A single bladed HAWT is the least widely used although they benefit by saving on materials. In order to balance the weight of the blade there is usually a counterbalance attached to the hub on the opposing side of the blade. Two bladed HAWTs may also save more materials than a three bladed HAWT and are more energy efficient than a single bladed HAWT. They also require no need for a counterweight. A three bladed HAWT will however capture more energy than either the single bladed or two bladed HAWT and it is for this reason they are the most widely used. Multi bladed HAWTs are mostly used as windmill water pumps. They are typically not used for generating electrical power. [15] See figure 2 for a side by side comparison.

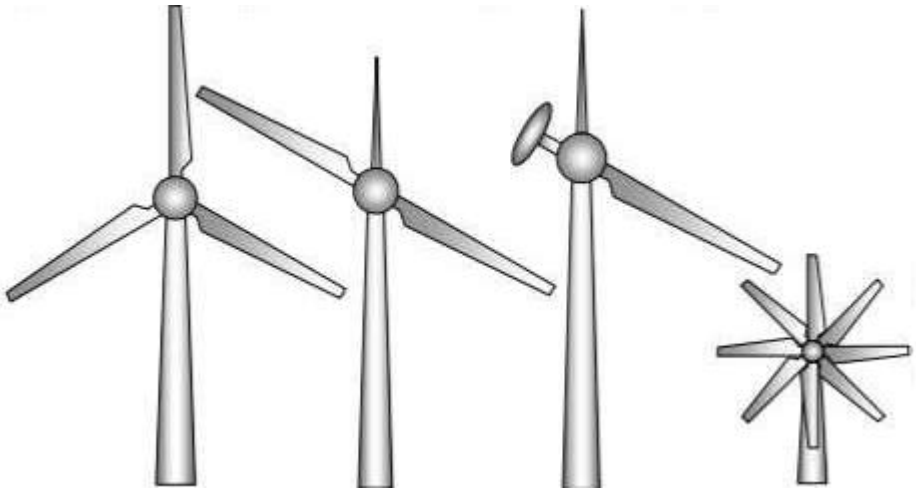

Figure 2: Comparison between triple, double, single, and multi bladed wind turbines. [16]

HAWTs can also be classified as upwind or downwind turbines. If the wind stream makes contact with the rotor before the tower it is known as an upwind wind turbine. These have an advantage of functioning in undistributed air flow. [12] The disadvantage of using an upwind wind turbine is the need for a 'yaw' system to control the direction the wind turbine faces. This is needed to prevent the turbine from turning downwind. Conversely, if the wind stream makes contact with the tower before the rotor it is a downwind wind turbine. These have the advantage of not requiring a yaw system since the wind will keep the rotor in the downwind configuration. These are however less efficient due to a wake formed by the tower causing uneven air loads on the blades. This also leads to larger fatigue damage on the blades. [13] See figure 3 for a side by side comparison.

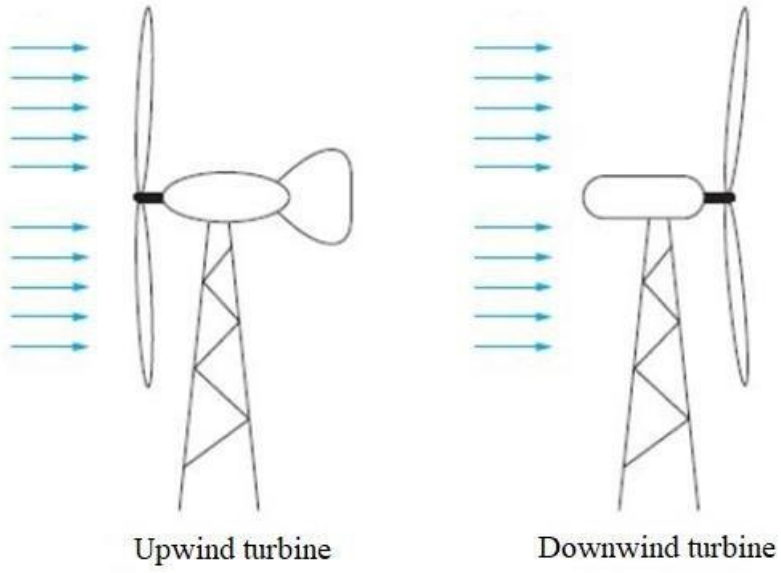

Figure 3: Comparison between upwind and downwind horizontal axis wind turbines. [17]

Most wind turbines manufactured and produced are three bladed HAWTs. [18] The main components of such a wind turbine are shown in figure 4. This can be separated into the rotor, which includes the rotor blades and the rotor hub; the nacelle which includes the gearbox, rotor break, generator, and yaw mechanism; and the tower. [19]

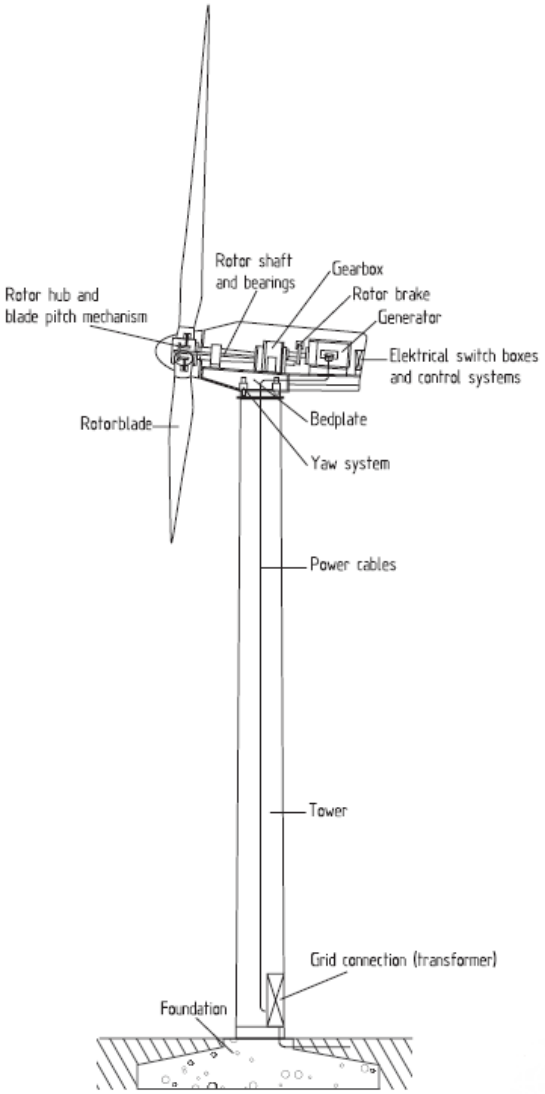

Figure 4: Components of a horizontal axis wind turbine. [18]

2.1.2 The wind turbine rotor

The wind turbine rotor is the most essential component of a wind turbine as it is what extracts the kinetic energy from an air stream. This energy gives the wind turbine rotor angular momentum which can then drive an electrical generator. The rotor consists of the hub and the wind turbine blades.

The hub connects the wind turbine blades to each other and to the nacelle. By doing so it is able to transfer loads in each of the blades to the drive train. The type of hub depends on forces and moments which are transmitted to the rotor. See figure 5 for a diagram of the hub.

Figure 5: Diagram of wind turbine hub [20]

Wind turbine blades can be made from a vast array of materials including wood, steel, carbon fibre and fibreglass. The properties of the blade depend strongly on the material used as well as the blade dimensions, operating wind conditions and stresses that arise from bending on the hub. Large scale wind turbine blades are typically constructed from glass-reinforced plastic (GRP), carbon fibre-reinforced plastic (CFRP), aluminium and steel. [21] A composite is created in order to achieve long, lightweight blades with high stiffness. For example, fibre glass wind turbine blades produce high stiffness, flexural strength, and shear resistance characteristics under extreme thermal and mechanical conditions. Some blades may also use high grade resins such as epoxy.

2.2 Aerodynamics

The aerodynamics of the wind turbine blades is the study of air forces on the wind turbine blades when air passes through. The qualities of a wind turbine blade that determine the aerodynamic interactions are the blade airfoil, twist, pitch, chord length and radius.

2.2.1 Airfoils

The airfoil of a wind turbine blade is simply a cross section of the blade, as shown in figure 6. It is the shape of this cross section that can create the mechanical forces necessary to move the wind turbine rotor due from the motion of air around the airfoil. The twist determines the angle at which the air stream makes contact with the blade airfoil at a given radius, while the pitch determines the angle the tip of the blade. The chord length determines the length of the airfoil at a given radius along the blade. The radius simply refers to the swept radius of the whole wind turbine rotor.

There are many types of airfoils available when designing a wind turbine blade. Figure 6 shows a diagram depicting a typical wind turbine airfoil from the National Advisory Committee for Aeronautics (NACA) series of airofils, showing all the significant parameters such as chord length *c*, the camber *f* and the position of maximum camber *(x_f)*.

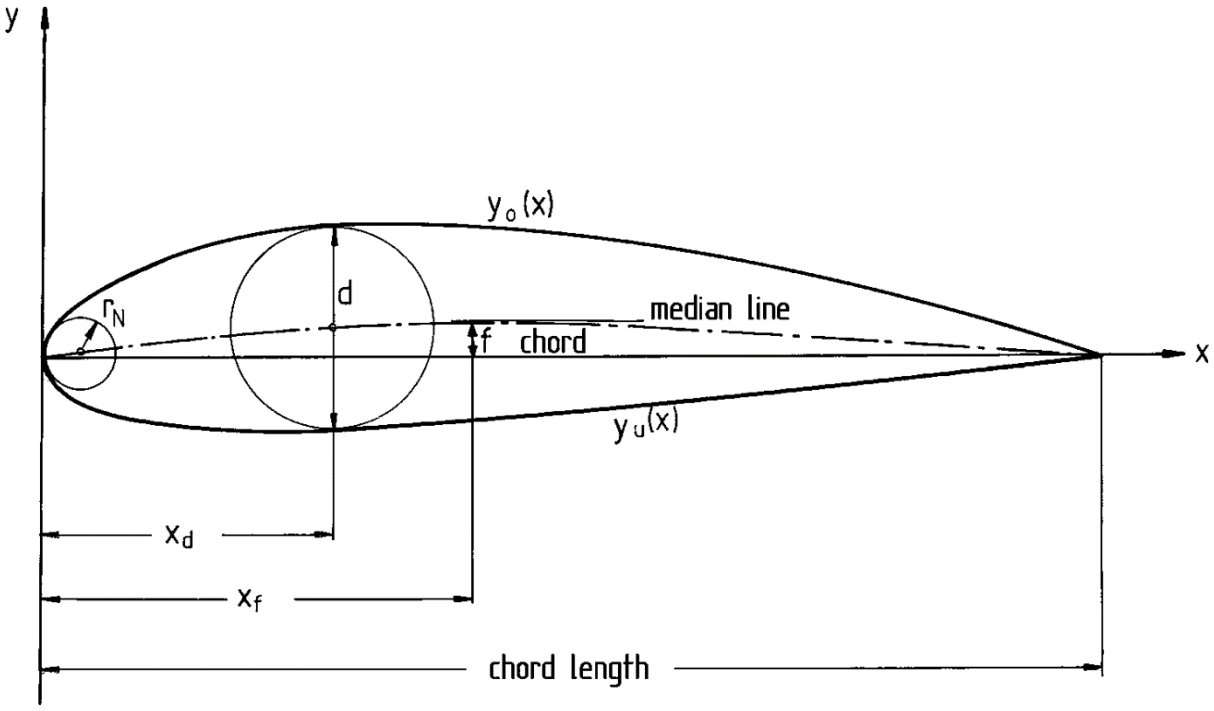

Figure 6: Geometric airfoil parameters of the NACA airfoil series [18]

NACA airfoils are listed with a four digit code which contains data on the airfoil geometry and partly on the aerodynamic properties. [18] The first digit contains information on the maximum camber to chord ratio. The second digit is the camber position in tenths of the chord length. The third and fourth digit are the maximum thickness to chord ratio in percentage. Airfoil coordinates are widely available to download online, usually with a chord length equal to 1. Figure 7 shows some examples of varying airfoil geometries.

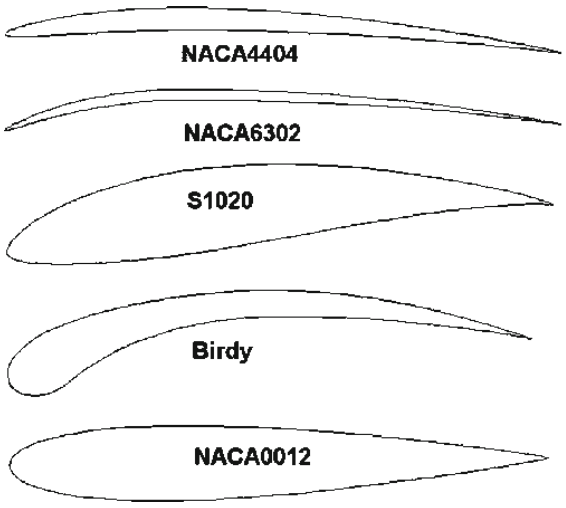

Figure 7: Examples of airfoil types [22]

Airfoils are designed for air to pass through the leading edge of the airfoil, as depicted on the left side of figures 6 and 7. The air then passes over the upper and lower surfaces of the airfoil. Due to the differences in shape between these two surfaces, the air will have to travel a different distance per unit time depending on if it is passing the upper surface or the lower surface i.e. air particles will move faster or slower on the upper or lower surfaces of the airfoil.

According to Bernoulli's theorem, the difference in the speeds across the upper and lower sides of the airfoil is created by the difference in pressures on these surfaces. These pressure differences create a net force *(R)* on the blade. [23] These are characterised as the lift force or drag force. The lift force is the component of the net force that is vertical with respect to the incoming air stream. The drag force is the component of the net force which is horizontal to the incoming air stream. The lift force is given by equation 1.

$$R_L = C_L \frac{1}{2} \rho A V^2 \quad (1)$$

Here C_L is the lift coefficient. $\rho A V^2$ represents the density of air, the projected airfoil area and the velocity of the undisturbed air squared. The drag force is given by equation 2.

$$R_D = C_D \frac{1}{2} \rho A V^2 \quad (2)$$

Here C_D is the drag coefficient. Figure 8 depicts a force diagram on an airfoil indicating lift and drag forces.

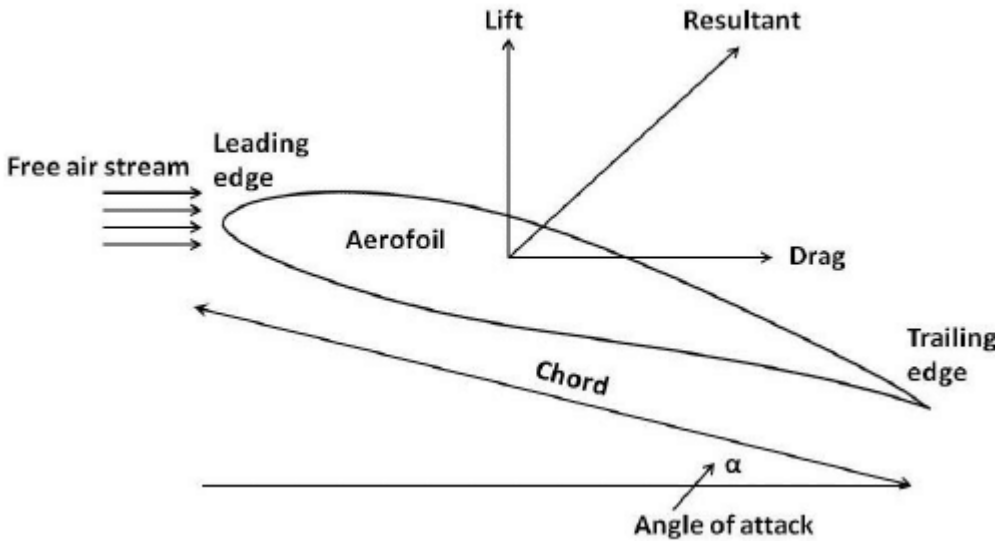

Figure 8: Forces on a wind turbine airfoil [24]

Lift and drag coefficients are typically measured in experiments known as wind tunnel experiments. Here, the lift and drag forces are measured by transducers located on the vertical and horizontal planes. [25] These coefficients depend on the angle of attack of the airfoil and so the experiments are usually done at a range of angles to generate a plot between the coefficient and the angle. This angle of attack is described by the twist at a given radius of a wind turbine blade, and the pitch.

2.2.2 Power and torque

The kinetic energy E_k of a given air stream can be described by the mass of air m and the velocity of the air stream V using equation 3:

$$E_k = \frac{1}{2}mV^2 \tag{3}$$

We can consider the volume of air to be described as a cylinder with the radius equal to the swept radius of the wind turbine rotor. The energy per second can be given by equation 4:

$$\dot{E_k} = \frac{1}{2}\dot{m}V^2 \tag{4}$$

Here, $\dot{m}$ is the change of mass per second which is given by equation 5:

$$\dot{m} = \rho AV \tag{5}$$

Here, ρ is the density of air. A is simply the cross sectional area of the cylindrical air stream, $A = \pi r^2$. Since power is defined as the energy per unit time, we get equation 6 for the power P of the wind passing through the rotor:

$$P = \dot{E_k} = \frac{1}{2}\dot{\rho A} V^3 \quad (6)$$

Since this is an ideal case, and it is not possible to extract all this energy, some of the kinetic energy is transferred to the rotor and the rest leaves the rotor by the wind. The amount of wind energy that is transferred from the wind to the wind turbine rotor is defined by the power coefficient C_P. This describes the efficiency of the wind turbine rotor and is given by equation 7:

$$C_P = \frac{2P_T}{\rho A V^3} \quad (7)$$

P_T is the power output of the wind turbine. There are many factors involved to determine the power coefficient including the number of wind turbine blades, the airfoil, pitch and twist. The torque of the wind turbine rotor may be determined by using equation 8 for the thrust force done by the wind turbine rotor:

$$F = \frac{1}{2}\rho A V^2 \quad (8)$$

From this we can now determine the torque to be shown in equation 9:

$$T = \frac{1}{2}\rho A V^2 r \quad (9)$$

Here r is the radius of the wind turbine rotor. Since this is again the ideal case, the real value of torque will be less than this value. We can express this real value by using a term known as the torque coefficient C_T. This is defined as the ratio between the real torque and the theoretical torque described in equation 9. This gives us the equation 10:

$$C_T = \frac{2T_R}{\rho A V^2 r} \quad (10)$$

In equation 10, T is the real torque of the wind turbine rotor.

One other value used to determine the efficiency of the interaction between the wind turbine rotor and the stream of wind is defined as the ratio between the velocity of the tip of the wind turbine rotor and the velocity of the stream of wind. This ratio is known as the tip speed ratio λ and is given by equation 11:

$$\lambda = \frac{r\omega}{V} \quad (11)$$

Here, ω is the angular velocity. This can also be expressed in terms if the torque coefficient and the power coefficient using equation 12:

$$\lambda = \frac{C_P}{C_T} \tag{12}$$

These values based on aerodynamic theories are very useful when designing a wind turbine rotor. The tip speed ratio for instance will depend on the function of the wind turbine. Wind pump rotors require a low tip speed ratio due to the high starting torque. On the other hand, electricity generating wind turbines require a high tip speed ratio due to the fast moving rotor. [25] The number of blades a wind turbine uses directly affects the tip speed ratio.

2.3 Loads on a turbine blade

There are numerous sources for loads present on a wind turbine at any given time. Since it is these loads that cause the stress required for fatigue failure to occur, we must study these loads in depth. The most significant of these is the aerodynamic loads due to the wind. These may be considered uniform, steady state air flow loads when the wind is in the direction of the turbine with a uniform distribution of wind speed across the rotor. Typically loads are unsteady and spatially non-uniform due to wind shear and cross winds, causing cyclic load changes on the rotor. There may also be, gravitational loads, inertial loads due to the dead weight of the turning rotor blades and stochastic loads caused by wind turbulence. [18] These loads can be determined by geographic and weather conditions as well as relative locations of a turbine in a heavily populated wind farm. Finally, there may be operational loads present at different operating states of the wind turbine. [25]

2.3.1 Uniform and steady state air flow

Assuming an even distribution of air across the rotor is a strong idealisation but it is useful for practical purposes when calculating the mean loading over a long period of time. In this case the aerodynamic loads present on a wind turbine blade can be described using equations 1 and 2 for the lift and drag forces. These forces are largely determined by the effective wind speed, which varies from the root of the blade to the tip when the rotor is in operation. This distribution of loads along the blade also varies significantly from the start up wind speed to the shutdown wind speed, due to the blades twist. The twist is designed for an optimal wind speed, and at higher wind speeds the flow separates in the blade sections near the hub causing the change in load distribution. [18]

2.3.2 Vertical wind shear

In reality, wind flow velocity is non uniform across the wind turbine rotor at any given time. This causes a much more complex variety of loads present. This however can be described by wind shear allowing us to approximate a more accurate solution for loading. Wind shear describes the change in wind velocity with respect to height. Wind typically moves much slower as it gets closer to the ground due to the resistance of the surface, whereas at greater heights wind is much freer to move quickly. This is depicted in figure 9.

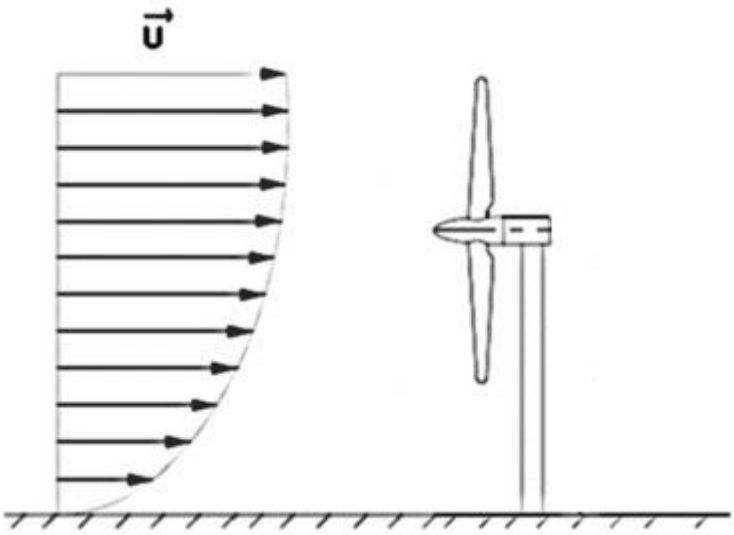

Figure 9: Vertical wind shear [26]

Wind shear can be approximately described using the power law. This is detailed in the following equation:

$$\frac{V_2}{V_1} = \left(\frac{h_2}{h_1}\right)^{\alpha} \tag{13}$$

Here, V_1 and V_2 represent the mean velocity at two given heights, h_1 and h_2. α is known as the shear coefficient. Vertical wind shear causes a cyclic change in loading as the wind turbine rotates around in a circle. This produces a peak loading every revolution when a wind turbine blade is pointed vertically upwards and a minimum loading when the blade is pointed downwards to the ground.

2.3.3 Wind turbulence stochastic loads

Incorporating wind turbulence into a loading calculation can prove to be challenging due to the stochastic introduction of wind velocities. Wind normally moves in all three directions, longitudinal, vertical, and lateral. [12] However, it is typical for most calculations to assume a one-dimensional fluctuation in wind speed in the longitudinal direction due to the difficult

nature of incorporating a second dimension. Spatial distribution of wind speeds along the swept rotor area in this longitudinal direction is much more significant as far as loading is concerned. [18] Wind turbulence is characterised as high frequency fluctuations with occasional sporadic high deviations in wind speed known as gusts, usually described by a gust factor. [27] While turbulence can be very challenging to model and predict, it does contribute significantly to wind fatigue, particularly to the rotor blades.

2.3.4 Gravitational and inertial loads

Gravitational loads for wind turbines become significant for large scale wind turbines. As the size of the turbine increases, so does its mass. The structures weight becomes a considerable factor when designing strong supports such as the tower or the hub.

Centrifugal loads are present while the wind turbine is in operation. These are not very significant in larger turbines with lower rotational speeds. [25] Centrifugal loads can also be used to counter act aerodynamic loads by a special trick known as coning. This is where the rotor blades are inclined at a small angle downwind such that the centrifugal load opposes the upwind direction of the aerodynamic loading. This can however be counter intuitive if the rotor is subject to strong gusts, causing wind direction to be momentarily reversed.

Gyroscopic loads are present in upwind wind turbines while the rotor is being yawed into the direction of the wind. If the rotor is yawed quickly these loads can be very significant but in most cases the rate of yaw is relatively low.

2.4 Computational methods

2.4.1 Finite element method (FEM)

FEM is a powerful numerical method is a numerical operation that is used to find a solution to a wide variety of engineering and physics problems. [28] These are typically problems involving stress analysis, heat transfer, electromagnetism, and fluid flow. In engineering there are a wide variety of complex problems for which we can’t achieve exact solutions. This may be due to complex governing differential equations. For these difficult problems we resort to numerical methods such as FEM.

FEM involves an integral of the differential equation over the model domain, which is divided up into individual elements connected by nodes. These elements are solved individually by defining approximate interpolation for each element, which are then placed

together to provide a solution for the entire model. [29] The division of the model in to differing elements is known as the mesh which can be shown in figure 10

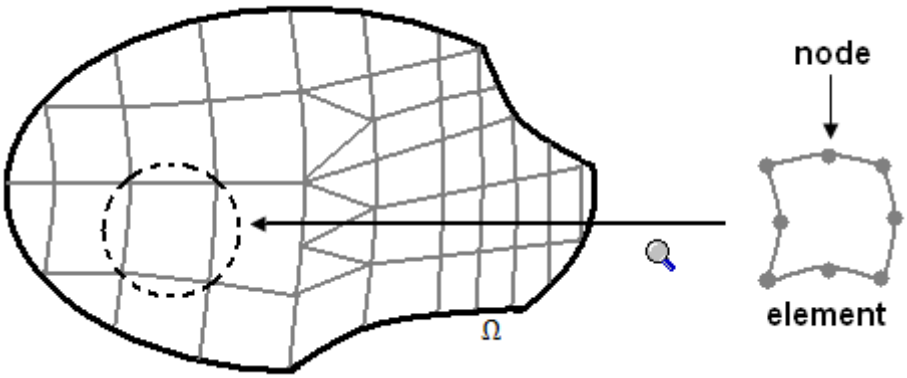

Figure 10: Mesh element example in two dimensions [30]

Once the mesh is finalised, there are several methods that can be used by FEM to generate a solution, such as direct formulation, minimum total potential energy formulation and weighted residual formulations. In general, an approximate continuous function is assumed for an element to represent its behaviour. Equations are then developed for every other element based on the solution. Finally, the elements are assembled back together to present the entire problem. From here, boundary conditions, initial conditions and loading may be applied to the problem to obtain solutions from a set of algebraic equations. [28]

2.4.2 Computational fluid dynamics (CFD)

CFD is used to predict and model fluid flow or heat transfer in a system. CFD methods are used in applications across the wind energy industry. As the wind energy continues to grow and potential wind farm sites become more and more scare, complex CFD calculations will be required to advance the industry further. [31]

CFD solves complex problems by using a using the model domain divided up into individual elements known as the mesh. From there the physical and chemical phenomena need to be modelled, fluid properties must be inputted the appropriate boundary conditions must be placed on cells that touch the boundary. [32] CFD simulations can be done using FEM to solve differential equations, however it is much more common to use the finite volume method (FVM) as the numerical method. FVM is a numerical method based on transport equations governing fluid flow and heat transfer. These governing equations are the continuity (conservation of mass, equation 14) and Navier-Stokes (Conservation of momentum, equation 15) equations, and are defined as follows:

$$\frac{\partial \rho}{\partial t} + \nabla \cdot \rho \overrightarrow{v_r} = 0 \quad (14)$$

$$\nabla \cdot (\rho \overrightarrow{v_r} \overrightarrow{v_r}) + \rho(2\overrightarrow{\omega} \times \overrightarrow{v_r} + \overrightarrow{\omega} \times \overrightarrow{\omega} \times \vec{r}) = -\nabla p + \nabla \cdot \tau_r \quad (15)$$

Here, $\overrightarrow{v_r}$ is the relative velocity and $\overrightarrow{\omega}$ is the angular velocity. p is momentum and ρ is density. τ_r is the viscous stress term, $2\overrightarrow{\omega} \times \overrightarrow{v_r}$ is the Coriolis effect term and $\overrightarrow{\omega} \times \overrightarrow{\omega} \times \vec{r}$ is the centripetal acceleration term. [32] CFD also has turbulence modelling capabilities using a model known as the k-ω SST model, which uses a modified Navier-Stokes equation known as the Reynolds averaged Navier-Stokes equation. [32]

2.5 Fatigue assessment analysis

In material science fatigue is the weakening of a material caused by cyclic loading that results in progressive and localised structure damage and the growth of cracks. If fatigue is considered a possible failure mode in a component then the fatigue strength of the material, the operating stress levels and the minimum cycles to failure must be considered as part of the design process.

Fatigue can be characterised as either being low cycle fatigue or high cycle fatigue depending on the number of stress cycles required before bringing a body to failure. [33] Low cycle fatigue usually occurs in less than 10,000 cycles whereas high cycle fatigue occurs thereafter.

The number of cycles to failure can be found for a material by using its *S-N* curve. This is a plot between number of cycles to failure *N* and the allowable stress amplitude *S* of a cyclic stress. There are currently numerous sources of available data for different material's *S-N* curves, as well as a methodology for approximating *S-N* curves. [34, 35]

3.0 Methodology

The methodology was split in to two large sections. Firstly, the model design was developed by defining the geometry of the wind turbine blade and the mesh for both the blade and the air around it. Time was spent to make sure this geometry was made as accurately as possible. Secondly, the simulations of various loads were introduced to the model. Initially a fluid flow model was simulated in order to achieve aerodynamic loads. In this model, a fluid flow, a static structural analysis and a modal analysis are required. The model geometry was constructed on ANSYS DesignModeler and would include just one wind turbine blade given the symmetry between the blades. Limits to the number of mesh elements on ANSYS student version also limited the volume of air to be simulated.

3.1 Model design

A wind turbine model was chosen at the beginning of this experiment to guide the computer model and act as a framework. Airfoil and twist coordinates were chosen from the NREL 5MW wind turbine as these specifications are widely available online. [36] This a un upwind, three bladed HAWT. More commercial wind turbines typically do not share airfoil and twist information as this would be confidential. The NREL wind turbine was then further modified to be closer to a commercial turbine model. Dimensions were modified according to available information regarding the Vestas V117 - 4.2MW model, changing the model maximum chord length and rotor radius. This model was chosen as it is a very modern turbine designed to be used in strong wind conditions, like the NREL wind turbine. [37] It is also currently being used for the current development of the Viking wind farm in the Shetland Islands, United Kingdom. Details of the hybrid model developed component dimensions can be found in table 1.

Table 1: Wind turbine blade geometry

Element	Radius (m)	Twist (°)	Chord length (m)	Airfoil type
1	1.393	13.308	3.046	Cylinder
2	2.662	13.308	3.046	
3	10.911	13.308	3.918	DU40 A17
4	14.718	11.480	4.000	DU35 A17
5	18.525	10.162	3.833	
6	22.333	9.011	3.653	DU30 A17
7	26.140	7.795	3.445	DU25 A17
8	29.947	6.544	3.223	
9	33.754	5.361	3.011	DU21 A17
10	37.562	4.188	2.800	
11	41.369	3.125	2.588	NACA64 A17
12	45.176	2.319	2.377	
13	48.983	1.526	2.165	
14	52.156	0.863	1.989	
15	54.694	0.37	1.794	
16	57.232	0.106	1.220	
17	58.501	0.106	1.220	

For this model the pitch was kept to 0°and the tilt was kept to 0°.

3.1.1 Geometry

These coordinates were carefully inputted in to DesignModeler generating 17 different cross sections of the wind turbine blade. With these cross sections defined, the skin/loft feature was then used to generate a smooth surface over each of the elements and a body was created. This can be seen in figure 11:

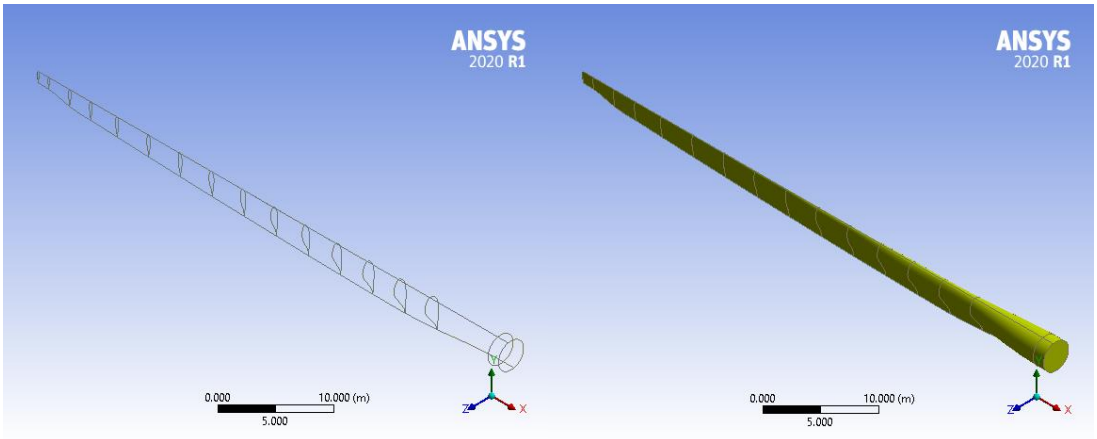

Figure 11: Blade skeleton (left) and blade body (right)

Two copies of this same blade were then generated. One of these will be used to model the mesh of the blade for FEA. A varying thickness was added to the FEA geometry of this model as a linear function from 0.15m to 0.005m, from the base to the tip of the blade. The second model will be used as a volume to be subtracted from a greater volume of air to be used with CFD. The volume of air was designed for the CFD calculation with a length of 270m, an upwind radius 120m and a downwind radius of 240m. It is designed as one third of a semi-circle as depicted in figure 12. This will then be extrapolated to create all three wind turbine blades.

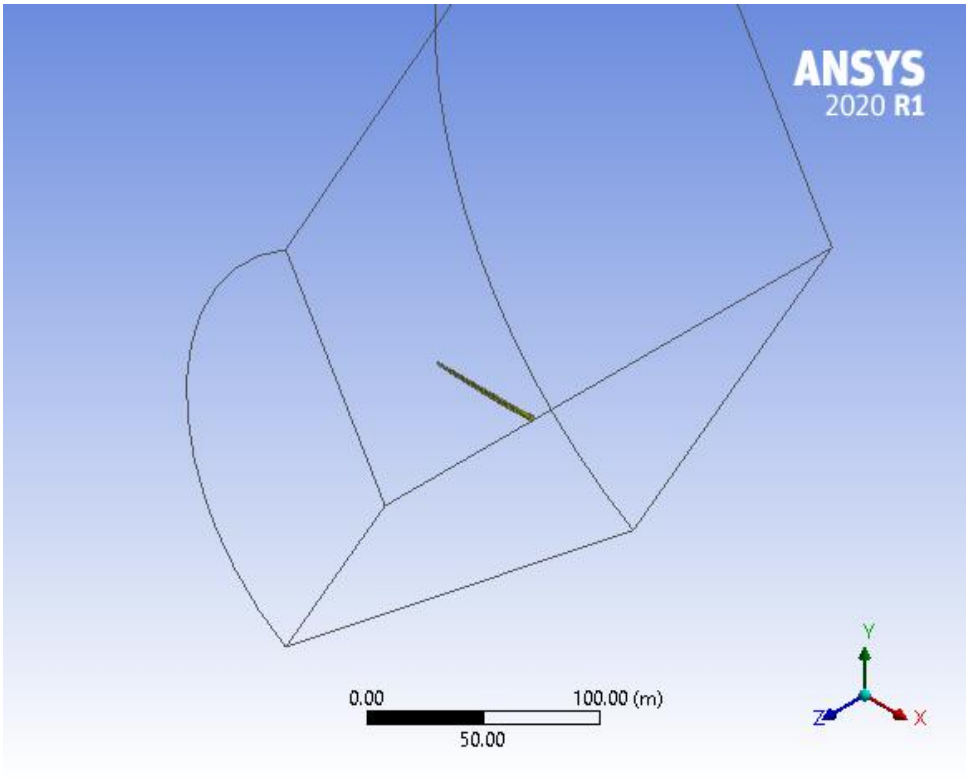

Figure 12: Fluid body geometry

3.1.2 Mesh

The fluid mesh was generated first since the results for the CFD calculations will be used for the FEM calculations. This process started with a default 3D mesh generated automatically by ANSYS fluent which gives a mesh with tetrahedral cells that are tailored to CFD calculations. The generated mesh contains adequate inflation and sizing to run our calculation, but smaller element sizes may be used to improve accuracy. Additional modifications to the mesh were made. 'Match control' was applied such that the nodes of two surfaces with quadrilateral faces match up. This is important when extrapolating the fluid geometry to 360°. The final mesh contains 42,378 nodes and 237,733 elements, which is within the limit of ANSYS student version. A cross section can be seen in figure 13.

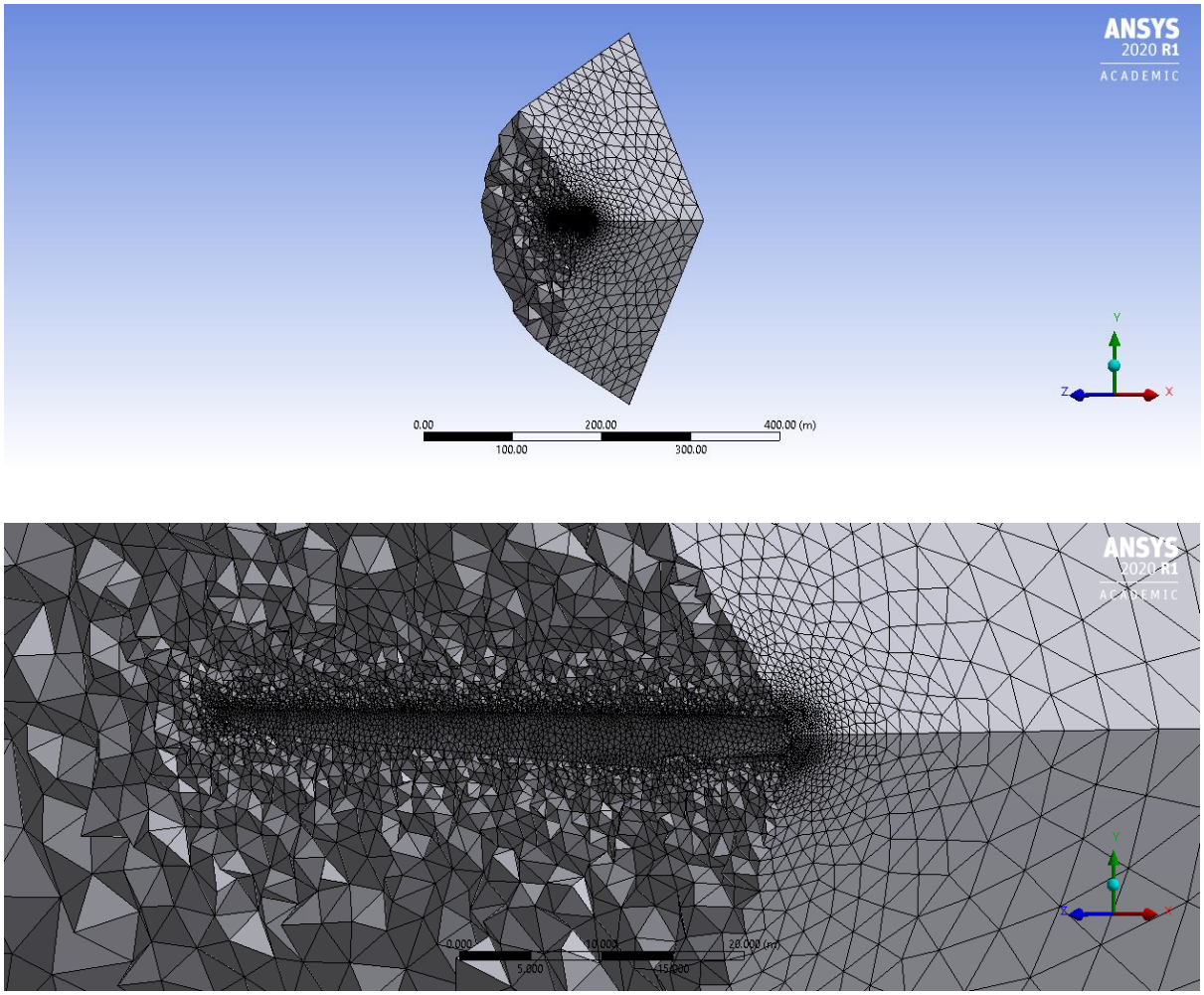

Figure 13: 3D cross section of fluid mesh

Secondly, the mesh for the blade was created for FEM calculations. This requires much less elements as it is treated as a hollow body with a small thickness. The process for meshing once again started with the default mesh generated automatically by ANSYS mechanical tailored for FEM calculations. A mapped face mesh was generated on the surface

to create quadrilateral elements. The final mesh contains 8,755 nodes and 8,507 elements, which is within the limit of ANSYS student version. A cross section can be seen in figure 14.

Figure 14: Blade mesh

To ensure good quality of the mesh produced a quick analysis of orthogonal quality and skewness was done. These are values that range between 0 and 1. In general, it is advised to keep the minimum orthogonal quality to be greater than 0.15 and the maximum skewness lower than 0.95. [38] Details of the final mesh metrics that satisfied these conditions are given int table 2

Table 2: Mesh metrics

Mesh metric	Blade	Fluid
Minimum orthogonal quality	0.417	0.186
Maximum orthogonal quality	1	0.993
Average orthogonal quality	0.997	0.753
Minimum skewness	0.00000874	0.000256
Maximum skewness	0.670	0.814
Average skewness	0.0412	0.246

3.2 Simulations

In order to carry out the simulations in our model we must first define material properties. The material properties for air are simply defined with the following values in table 3.

Table 3: Properties of air

Property	Value
Density (kg/m^3)	1.225
Viscosity (kg/m·s)	1.789×10^{-5}

The properties of the wind turbine blade were then chosen based upon a database found on wind turbine blades composites. [39] For this analysis the blade design was to be made of a fibre glass-epoxy composite material. These properties assume material is isotropic and are summarised in the table 4.

Table 4: Properties of fibre glass-epoxy composite material

Property	Value
Density (kg/m^3)	2,600
Young's modulus (GPa)	85
Poisson's ratio	0.23
Shear modulus (GPa)	36
Ultimate tensile strength (GPa)	2.05

Given the variable thickness of the wind turbine blade outlined in the geometry section, we can compute the mass of the wind turbine blade to be 88,531kg.

3.2.1 CFD

CFD simulations were first carried out to determine the air flow and the loads these impose on the wind turbine blade. The CFD model is set up by defining the governing equations and boundary conditions within ANSYS fluent.

Settings were modified to carry out a steady simulation using the pressure based solver. Model settings were modified to use the k-ω SST model. This simulation must be carried out in the rotated frame of reference by enabling 'frame rotating' and inputting the blade rotational velocity to be -1.80rad/s defined around the positive Z-axis. This is equal to

approximately 17.5RPM which is the upper limit of the rotor speed as specified by the Vestas 117 data sheet. [37]

Boundary conditions are then defined. The inlet surface of the fluid and the outer curved surface of the fluid are given air velocities of -23m/s in the Z-direction. This is the re-cut in wind speed for the specified wind turbine indicating it's the highest stable operating wind speed. The turbulent intensity is set to 5%. The turbulent viscosity ratio is set to 10. The outlet of the fluid is given a pressure 101,325Pa which is equal to 1atm. Next, the two match controlled surfaces are set as interfaces connecting to each other.

Finally, the settings for the solution were set for high accuracy increasing the change for the solution to converge. The pressure-velocity coupling scheme was set to 'coupled', the spatial discretization pressure was set to 'standard', 'pseudo transient' and 'high order term relaxation' were turned on. The Residuals for velocity and continuity were set to 10^{-6} to ensure the calculation doesn't stop before converging. The integral static pressure is set to be monitored so one can see in real time if the solution is converging. The number of steps was set to 1,500, the settings were initialized, and the calculation was run.

3.2.2 FEM

FEM calculations were carried out to complete a static structural analysis and a modal analysis within ANSYS mechanical. Default static structural simulation settings were first loaded. The blade was given a rigid node at the base to simulate the assumed effect of having the blade be rigidly connected the hub. The blade was then given the same rotational velocity of 1.80 rad/s in order to calculate centripetal loading. 'Large deflection' setting was turned on to simulate the stress stiffening effect due to the fast spinning blade. The pressure loads from the CFD calculation were then simply imported to ANSYS mechanical. The calculation was run and ANSYS will automatically perform the calculation by forming the stiffness matrix for each element to get nodal displacements. From the nodal displacements, ANSYS can work out equivalent stress, force reactions and moment reactions.

A modal analysis was also carried out using the same rigid node and rotational velocity to determine the first six modes. The frequency for the first mode was then checked to determine if a harmonic response analysis is required. If the time required to apply a load is greater than three times the natural period, a dynamic response analyses is not required as the effects are negligible. [40]

3.2.3 Fatigue assessment analysis

The methodology used in carrying out a fatigue analysis is similar to the procedure used in the European Pressure vessel code and the SAE design handbook. [41, 42] Areas of high stress are located within the FEM model results file. Specifically, these include the maximum von Mises stress (S_{vm}), principal tensile stress (S_1) and principle compressive stress (S_3).

Using equation 16 the appropriate von Mises stress amplitude σ_a is then calculated based on the actual von Mises stress found from the FEM results.

$$\sigma_a = \frac{S_{vm}}{2} \tag{16}$$

This equation is used when the load starts at zero, rises to a peak and falls back to a minimum stress at zero as it adjusts the amplitude to cycle around the mean stress. If the mean stress is tensile we must modify the amplitude further using equation 16.

$$\sigma_{eqv} = \sigma_a \left[\frac{Su}{Su - \left(\frac{S_1+S_2+S_3}{2}\right)} \right] \tag{17}$$

Here, S_u is the ultimate stress of the material. The term $\left(\frac{S_1+S_2+S_3}{2}\right)$ is the mean stress using the first, second and third principal stress. This is based on the Goodman diagram which assumes that a compressive stress does not affect fatigue strength. [43] This modified von Mises stress is then used, with the appropriate notched *S-N* curve to calculate predicted cycles to failure.

4.0 Results and discussion

In analysing the results, one must first determine if results have converged sufficiently. The first step is to ensure mass is adequately balanced between the inlet, outer surface and the outlet. The mass flow rate at each of these surfaces is summarised in table 5 below

Table 5: Mass flow rate

Fluid surface	Value (kg/s)
Inlet surface	422,841.22
Outer surface	1,273,811.2
Outlet surface	-1,696,652
Net	-0.1128356

These were found to be adequately balanced indicating the model is good. The next step is to study the convergence of the integral static pressure. This is shown in figure 15 as seen where the integral static pressure converges at around -335,000Pa.

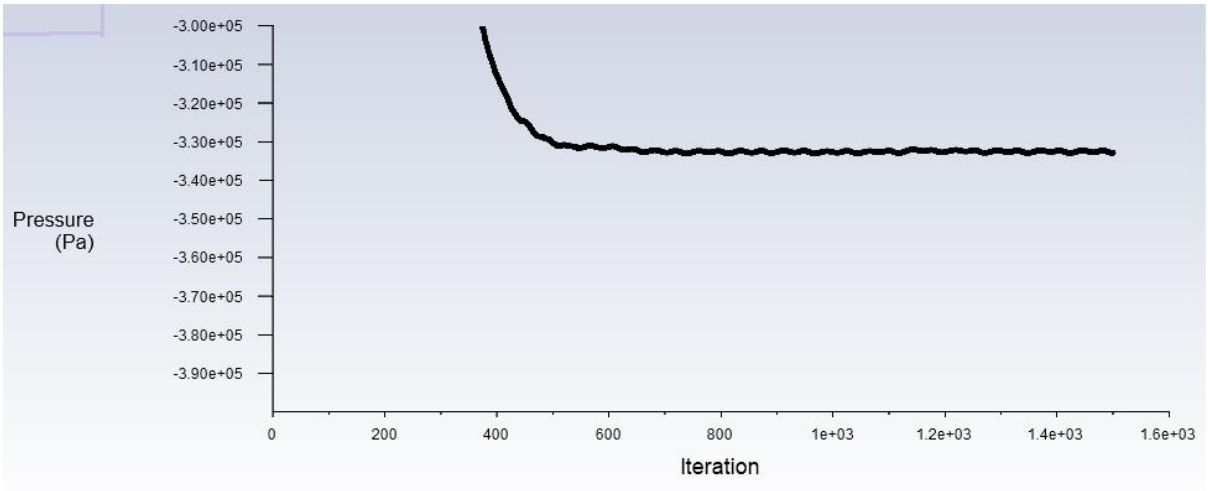

Figure 15: Convergence of integral static pressure

4.1 Fluid flow analysis

Results for CFD can be visualised and analysed using the program CFD-Post. Here we can visualise the complete triple bladed wind turbine rotor. Figure 16 shows this with vector arrows representing the tangential velocity of the wind turbine rotor varying along the radius. The legend shows a maximum velocity of 105.3m/s.

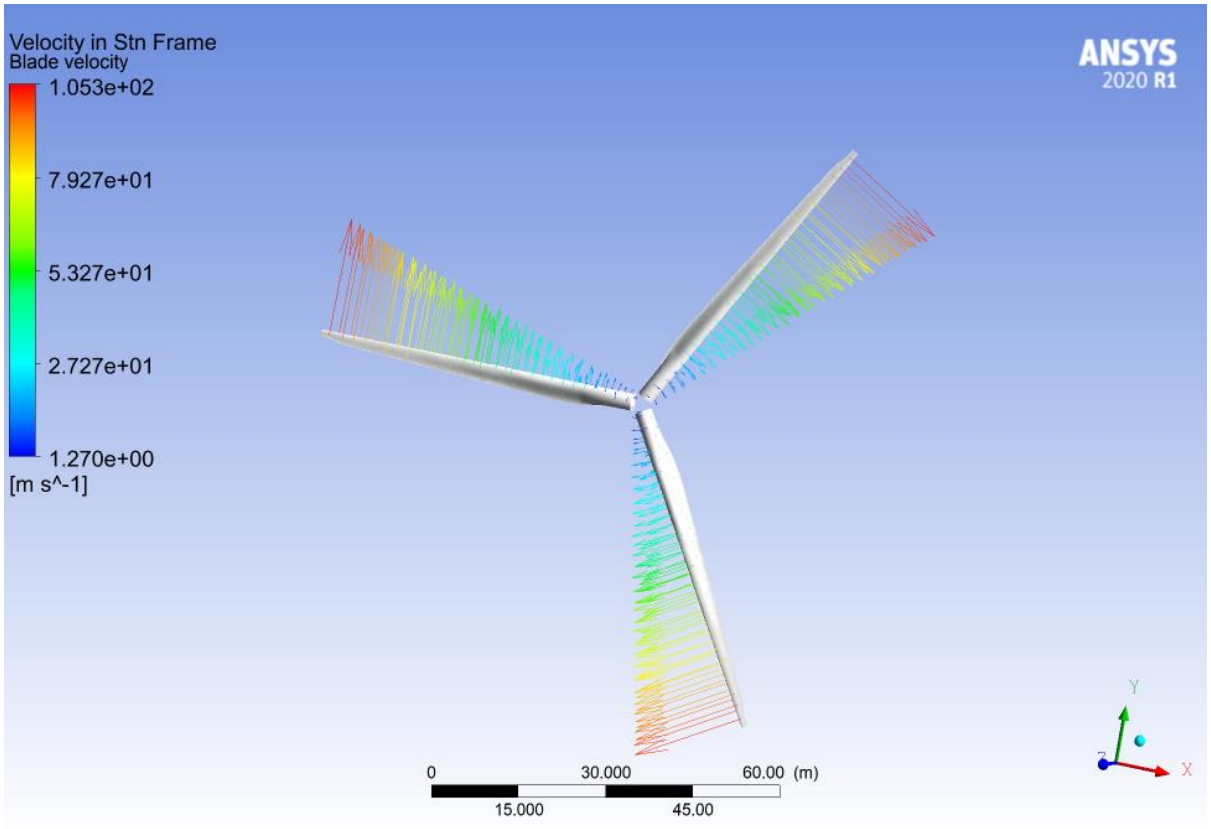

Figure 16: Velocity vectors of wind turbine rotor

Next we can visualise the velocity streamlines of the wind as it passes through the wind turbine rotor. These can be seen in figure 17 and 18. As we can see the velocity at the inlet is equal to the specified 23m/s. There is then a clear drop in velocity behind the wind, which is shown figure 19. This is due to the wake behind the wind turbine blade. Finally, there is also an increase in velocity around the wake. This can be described by a balance in momentum.

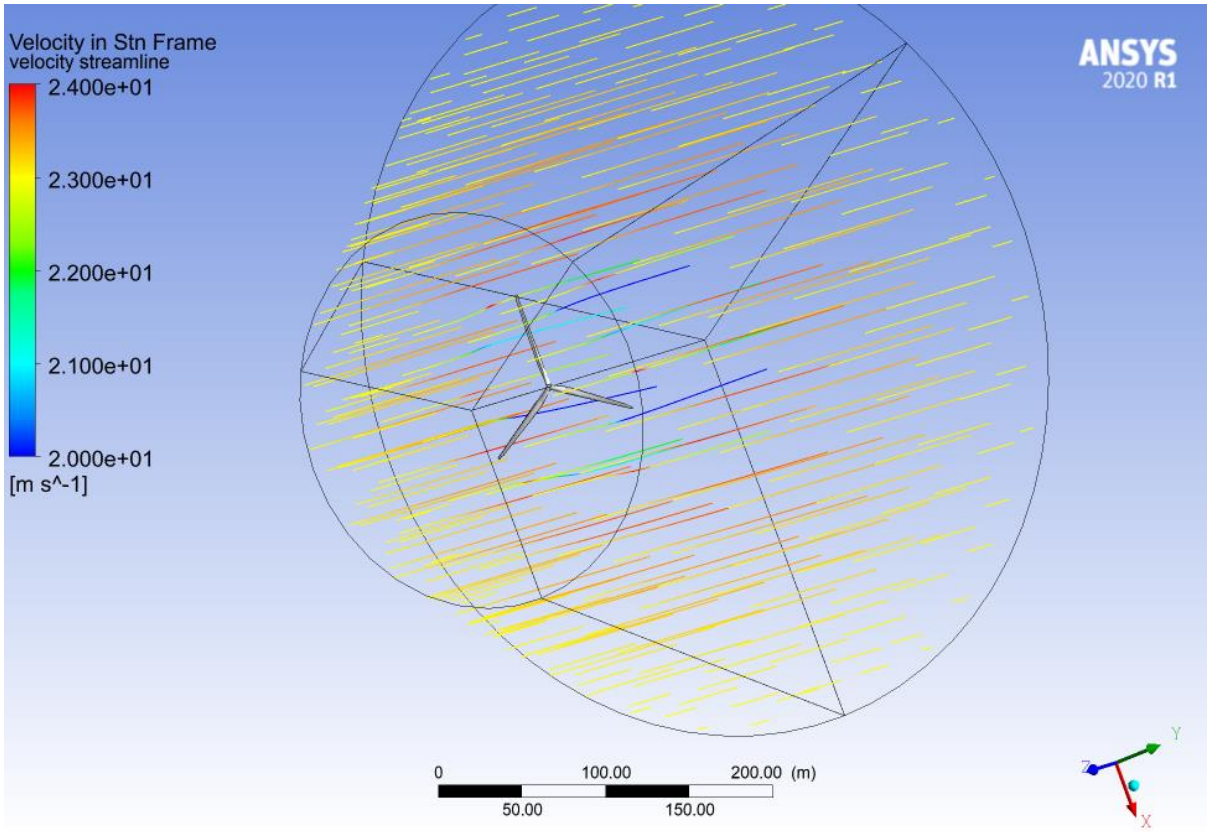

Figure 17: Velocity streamlines of wind for full model

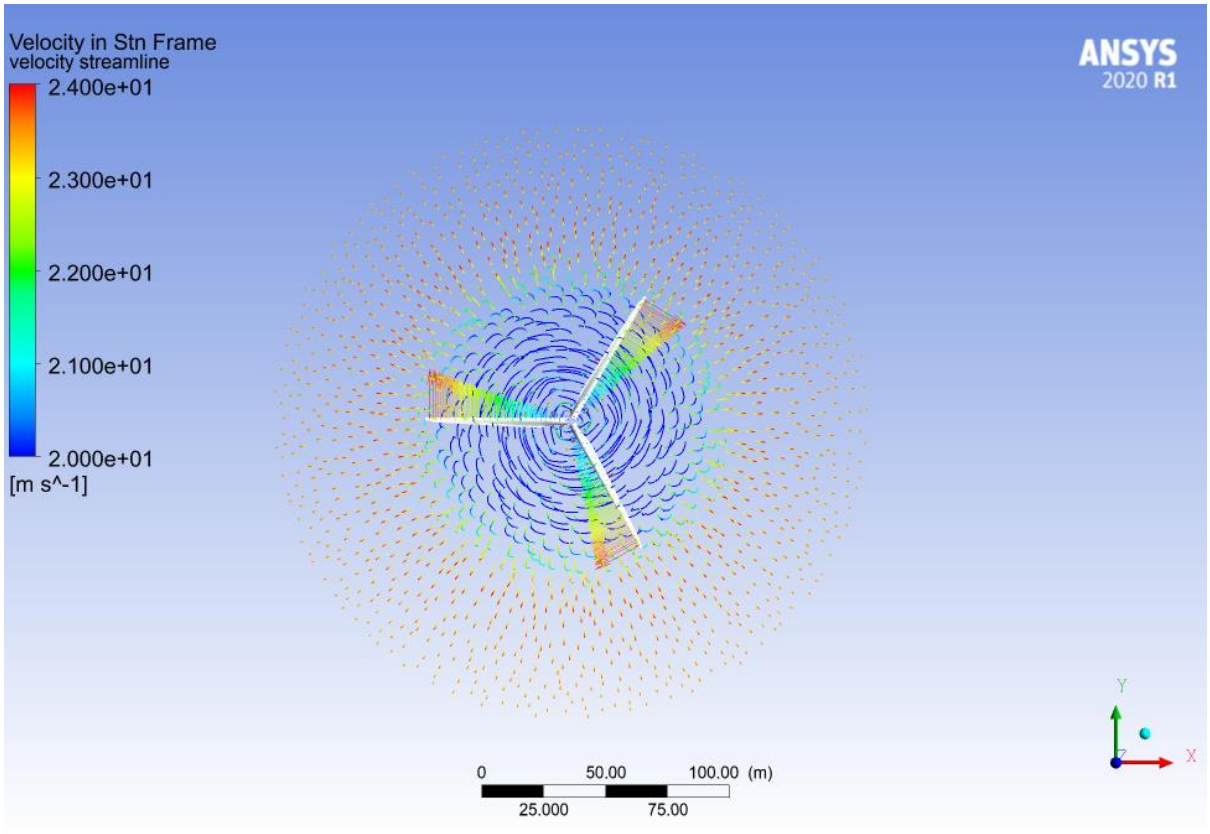

Figure 18: Velocity streamlines of wind with velocity vector of the wind turbine rotor

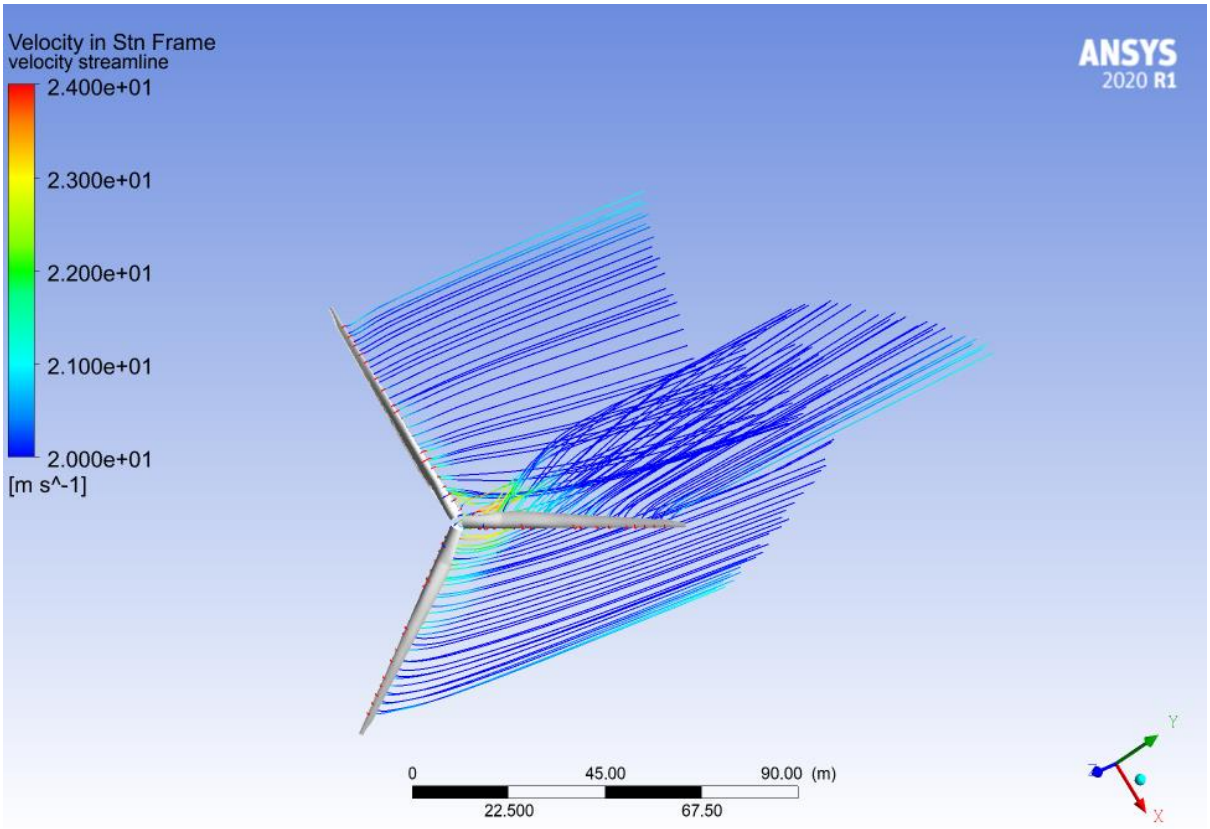

Figure 19: Velocity streamlines of wind behind the blade.

Next we can look at the pressure contours on the blade. These are shown in figure 20 and 21. Here we can see that the maximum pressure on the front and back of the blade are different, and the back surfaces of the blades experience a pressure that is much higher in magnitude. This pressure difference creates the lift force required for the wind turbine to rotate, since there is a component of this lift force that is in the plane of rotation. The component of lift that is parallel with the direction of incoming wind is what creates deflection of the blade, as will be studied in the static structural analysis.

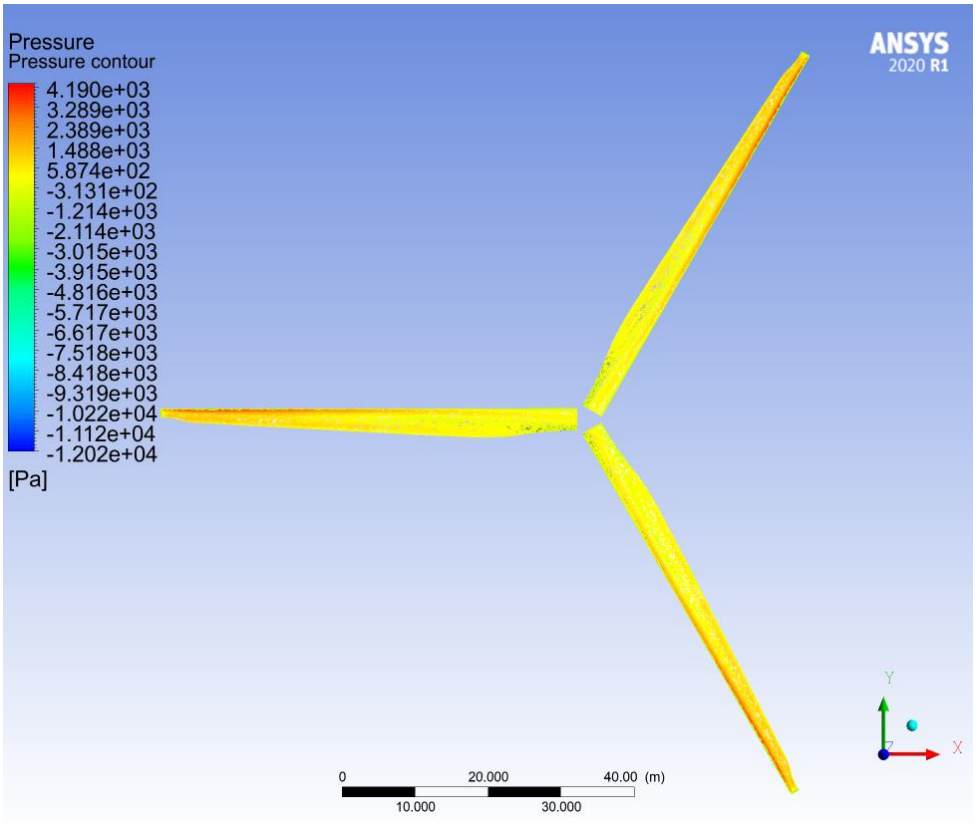

Figure 20: Pressure contours on the front of the blades

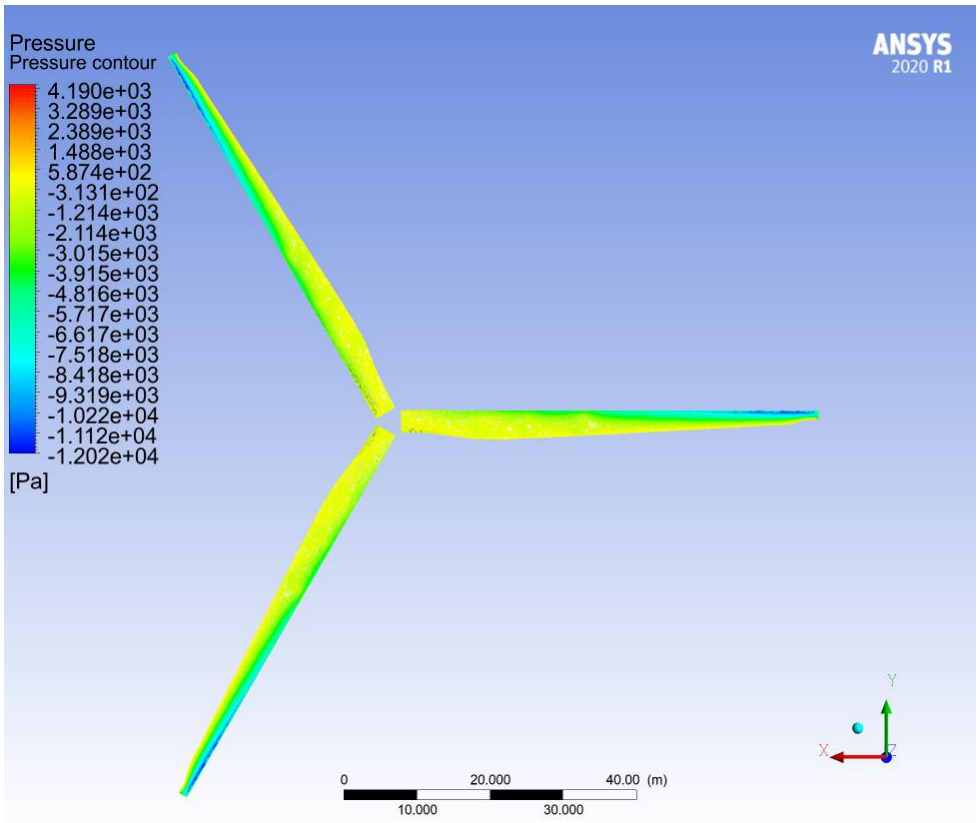

Figure 21: Pressure contours on the back of the blades

4.2 Static structural analysis

The first result studied within the structural analysis is the total deformation of the wind turbine blade. This is shown in figure 22 with the shadowed blade showing the original undeformed wind turbine blade.

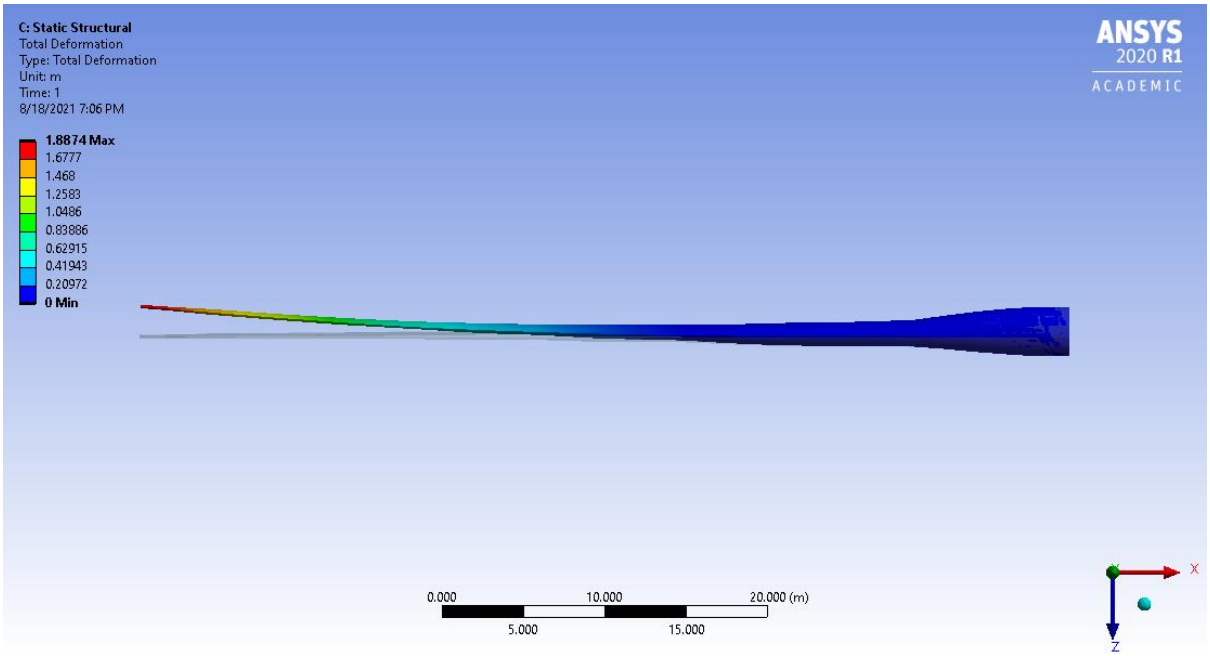

Figure 22: Deformed wind turbine blade

The deformation shown in figure 22 is to scale with the length of the blade. This data tells us the total deformation under these conditions is a maximum displacement of 1.8874m at the tip of the blade, in the direction of the wind. This is accurate to what happens in large wind turbines under high wind speeds.

The force reaction and moment reaction calculated are given as vectors. This is summarised in table 6.

Table 6: Force and moment reaction vectors

	Force reaction (N)	Moment reaction (Nm)
X-axis	5,232,000	356,950
Y-axis	-83,791	16,350,000
Z-axis	461,920	3,267,900
Total	5,253,000	16,677,000

In table 6 we can see that the largest component of the force reaction is in the X-axis. This is attributed to the centripetal acceleration of the rotating blade. The majority of the reaction bending moment is about the Y-axis due to how the blade is deforming.

We can validate our results be hand calculating the radial force. Given the mass of the wind turbine blade to be 88,531kg and the centre of mass to be at $Y = -18.294$, we can say

$$F = -m\frac{(\omega r)^2}{r} = -(88{,}531)(-1.80)^2(-18.294) = 5{,}247{,}459\ N$$

This value agrees with the ANSYS calculation with just a 3% difference.

4.3 Modal analysis

The first six mode frequencies from the modal analysis were found. These are summarised in table 7 along with the maximum deformation.

Table 7: First six modes of the turbine blade

Mode	Frequency (Hz)	Maximum deformation (m)
1	1.0236	0.02487
2	2.3442	0.02407
3	2.6771	0.02266
4	4.9117	0.03448
5	7.3539	0.026434
6	7.8855	0.035795

It was found that the natural period of the structure is 0.9769s. This is much smaller than the period of the turbine moving at 1.80rad/s, having a period of 3.49s. For this reason, it was considered arbitrary to conduct a harmonic response analysis. Figure 23 shows the mode shapes corresponding to each of the modes in table 7.

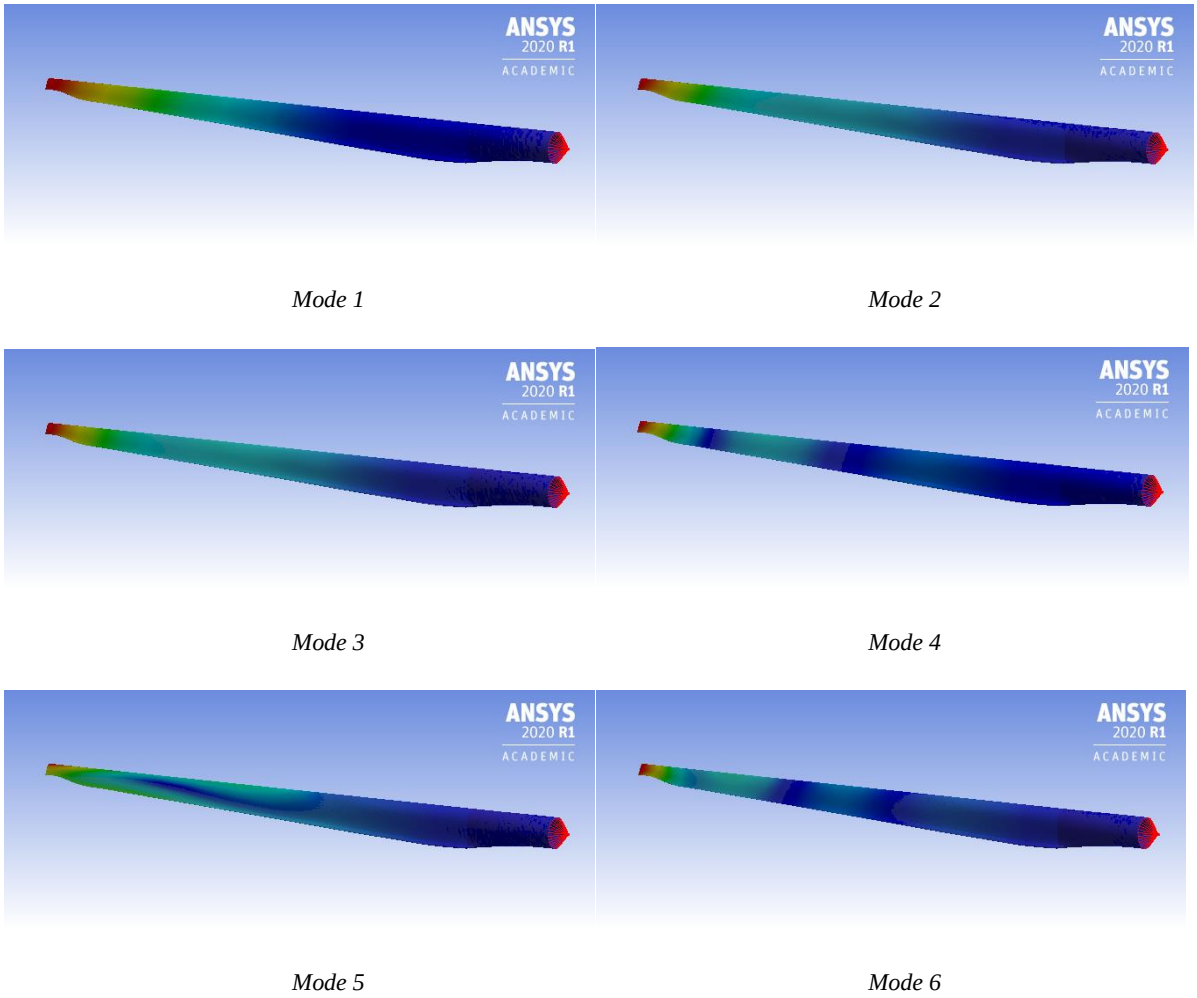

Mode 1 *Mode 2*

Mode 3 *Mode 4*

Mode 5 *Mode 6*

Figure 23: First six mode shapes of the wind turbine blade

The mode shapes shown represent the total deformation, with the maximum deformation shown in red and the minimum deformation shown in blue.

4.4 Fatigue assessment analysis

The nodes of maximum von Mises stress, principal tensile stress and principal compressive stress were found on the model and are summarised in table 8. The modified stress amplitude was also calculated for each of these nodes using equation 17, using the ultimate tensile strength shown in table 4 of 2.05 GPa.

From these equivalent values for the stress amplitude, we can see the maximum stress amplitude occurs at node 12. To determine the number of stress cycles of this magnitude before failure we must use an *S-N* curve for a glass-epoxy composite material. Figure 24 below shows an appropriate ε-N curve for such a material, with a Young's modulus of 29.6GPa. [44]

Table 8: Summary of maximum stress values

Node	S_{vm} (Pa)	S_1 (Pa)	S_2 (Pa)	S_3 (Pa)	σ_{eqv} (MPa)
12	5.1356×10^8	3.2376×10^8	514.5	-1.950×10^8	2.7879×10^8
7998	4.5163×10^8	4.4473×10^8	10,150	-4.6282×10^6	2.5296×10^8
3008	1.1014×10^8	1.3289×10^8	5.6512×10^7	6.6246×10^6	5.7835×10^7

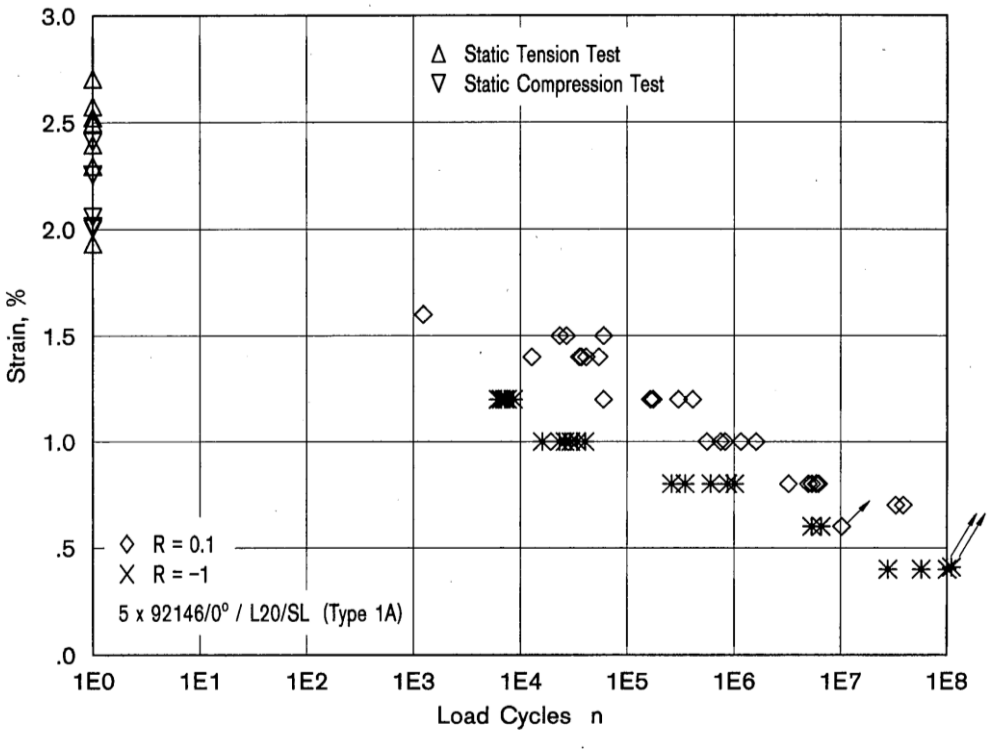

Figure 24: ε-N curve for glass-epoxy composite material [44]

In order to study the curve, one must convert the equivalent stress amplitude calculated into a strain percentage value using Young's modulus using equation 18 as the relationship between stress and strain.

$$E = \frac{\sigma}{\varepsilon} \tag{18}$$

This gives a maximum equivalent strain at node 12 to be 0.32%. According to figure 24, this means we can expect the number of load cycles before failure N ≈ 100,000,000. This is found to be a relatively high value and may be attributed to the decision to use pure fibre glass-epoxy composite material.

5.0 Conclusions

In conclusion, a wind turbine blade has been designed and modelled after current rotor blade specifications, and the structural integrity of the blade was successfully analysed. Overall, it was found that the experiment was quite effective.

The methodology for the blade design consisted of researching material specifications, geometry specifications as well as wind turbine airfoils, then, using a CAD program to draw the blade in three dimensions for use in simulations.

CFD calculations were performed using the CAD model. This proved successful as one was able to visualise the wind speed variations due to the wake behind the blade as well as the pressure contour across the blade due to the oncoming wind.

Further analysis was carried out on the structural integrity of the wind turbine blade. This included a visualisation of the deformation of the blade due to the pressure contours. The force reaction and moment reaction vectors were also calculated.

A modal analysis was carried out on the blade as well as a simple fatigue assessment analysis. The number of cycles to failure for our given load was calculated and was found to be quite high, indicating a long lifespan for the wind turbine blade.

While one has only scratched the surface on fatigue analysis and structural integrity, it was felt that the simulations used, and the results found could be very useful in making design decisions for wind turbine blades.

5.1 Further work

The information gathered in this report is limited to an analysis of just one wind turbine model, with limited data available and limited computer power. The immediate next step for this model is to carry out a mesh refinement analysis in both the CFD model and the FEM model. A finer mesh improves accuracy of the model at the expense of computing power but is a necessary step when validating the mesh. The ANSYS student version is limited to only 512,000 elements and nodes in a CFD model, and 32,000 elements and nodes in a FEM model, so a full version of ANSYS is needed to show convergence of the numerical solution with respect to the number of elements in the mesh.

While the purpose of this decision is to create a focus on modelling and designing for blade with limited available data, the methods must be validated across a wider range of wind turbine models and characteristics. Within the studied model, one might wish to study a wider variety of rated wind speeds and rotational velocities. Blade material properties may be modified to represent CFRP, GRP, steel, aluminium, or any composite material. The model geometry may be tested with varying radii, twist, pitch, tilt and airfoil selection to achieve a more accurate representation of a given wind turbine model. One may also choose to model the hub, nacelle, and tower for structural integrity.

Finally, a wider variety of analysis may be introduced to the model. These could include gravitational loads, gyroscopic loads, and non-uniform loads. A transient analysis of the turbine may also be done over a period of time to reflect potential changes in wind speed and turbulence, and how this might impact fatigue.

6.0 References

[1] I. B. Vasi, *Winds of change: The environmental movement and the global development of the wind energy industry*. Oxford University Press, 2011.

[2] M. Sathyajith and G. S. Philip, *Advances in wind energy conversion technology*. Springer Science & Business Media, 2011.

[3] Y. Zhou, P. Luckow, S. J. Smith, and L. Clarke, "Evaluation of global onshore wind energy potential and generation costs," *Environmental science & technology*, vol. 46, no. 14, pp. 7857–7864, 2012.

[4] C. C. Ciang, J.-R. Lee, and H.-J. Bang, "Structural health monitoring for a wind turbine system: a review of damage detection methods," *Measurement science and technology*, vol. 19, no. 12, p. 122001, 2008.

[5] C. W. Kensche, "Fatigue of composites for wind turbines," *International journal of fatigue*, vol. 28, no. 10, pp. 1363–1374, 2006.

[6] R. P. L. Nijssen, "Fatigue life prediction and strength degradation of wind turbine rotor blade composites," *Contractor Report SAND2006-7810P, Sandia National Laboratories, Albuquerque, NM*, 2006.

[7] P. Caselitz and J. Giebhardt, "Rotor condition monitoring for improved operational safety of offshore wind energy converters," *J. Sol. Energy Eng.*, vol. 127, no. 2, pp. 253–261, 2005.

[8] B. Le and J. Andrews, "Modelling wind turbine degradation and maintenance," *Wind Energy*, vol. 19, no. 4, pp. 571–591, 2016.

[9] B.-H. Han, D.-J. Yoon, Y.-H. Huh, and Y.-S. Lee, "Damage assessment of wind turbine blade under static loading test using acoustic emission," *Journal of Intelligent Material Systems and Structures*, vol. 25, no. 5, pp. 621–630, 2014.

[10] P. C. Guerrero, S. D. Mancini, and C. M. Toubia, "Caracterização e reciclagem qumica via pirólise de resduos da fabricação de pás eólicas," *Holos Environment*, vol. 11, no. 2, pp. 147–157, 2011.

[11] P. S. Oliveira, M. L. P. Antunes, N. C. da Cruz, E. C. Rangel, A. R. G. de Azevedo, and S. F. Durrant, "Use of waste collected from wind turbine blade production as an eco-friendly ingredient in mortars for civil construction," *Journal of Cleaner Production*, vol. 274, p. 122948, 2020.

[12] W. Tong, *Wind power generation and wind turbine design*. WIT press, 2010.

[13] J. G. McGowan and S. R. Connors, "Windpower: a turn of the century review," *Annual Review of Energy and the Environment*, vol. 25, no. 1, pp. 147–197, 2000.

[14] E. Kumara, N. Hettiarachchi, and R. Jayathilake, "Overview of the vertical axis wind turbines," *Int. J. Sci. Res. Innov. Technol*, vol. 4, pp. 56–67, 2017.

[15] J. Earnest and T. Wizelius, *Wind power plants and project development*. PHI Learning Pvt. Ltd., 2011.

[16] K. WOLNIEWICZ, W. KUCZYNSKI, and A. ZAGUBIEN, "Evaluation of wind resources for horizontal and vertical wind turbine,"

[17] M. Yassine Kebbati, "Design, modelling and control of a grid-connected hybrid pv-wind system (case study of adrar)," Master's thesis, 2018.

[18] E. Hau, *Wind turbines: fundamentals, technologies, application, economics*. Springer Science & Business Media, 2013.

[19] J. F. Manwell, J. G. McGowan, and A. L. Rogers, *Wind energy explained: theory, design and application*. John Wiley & Sons, 2010.

[20] E. L. Secco, A. Nagar, C. Deters, H. Wurdemann, H.-K. Lam, and K. Althoefer, "A neural network clamping force model for bolt tightening of wind turbine hubs," in *2015 IEEE International Conference on Computer and Information Technology; Ubiquitous Computing and Communications; Dependable, Autonomic and Secure Computing; Pervasive Intelligence and Computing*, pp. 288–296, IEEE, 2015.

[21] M. Hansen, *Aerodynamics of wind turbines*. Routledge, 2015.

[22] W. B. Tay and K. B. Lim, "Analysis of non-symmetrical flapping airfoils," *Acta Mechanica Sinica*, vol. 25, no. 4, pp. 433–450, 2009.

[23] N. F. Smith, "Bernoulli and newton in fluid mechanics," *The Physics Teacher*, vol. 10, no. 8, pp. 451–455, 1972.

[24] D. C. Panigrahi and D. P. Mishra, "Cfd simulations for the selection of an appropriate blade profile for improving energy efficiency in axial flow mine ventilation fans," *Journal of Sustainable Mining*, vol. 13, no. 1, pp. 15–21, 2014.

[25] S. Mathew, *Wind energy: fundamentals, resource analysis and economics*, vol. 1. Springer, 2006.

[26] G. Kavari, M. Tahani, and M. Mirhosseini, "Wind shear effect on aerodynamic performance and energy production of horizontal axis wind turbines with developing blade element momentum theory," *Journal of Cleaner Production*, vol. 219, pp. 368–376, 2019.

[27] W. Frost, B. Long, and R. E. Turner, "Engineering handbook on the atmospheric environmental guidelines for use in wind turbine generator development," tech. rep., Tennessee Univ., Tullahoma (USA). Space Inst.; National Aeronautics and â€¦, 1978.

[28] S. Moaveni, *Finite element analysis theory and application with ANSYS, 3/e*. Pearson Education India, 2011.

[29] A. Ismail-Zadeh and P. Tackley, *Computational methods for geodynamics*. Cambridge University Press, 2010.

[30] H. Policarpo, *Analytical, Numerical and Experimental Study of the Dynamical Response of Helicoidal Springs and Periodic Bars, 2008*. PhD thesis, MSc Thesis, Instituto Superior Técnico, Universidade Técnica de Lisboa, Portugal.

[31] Y. Bazilevs, M.-C. Hsu, I. Akkerman, S. Wright, K. Takizawa, B. Henicke, T. Spielman, and T. Tezduyar, "3d simulation of wind turbine rotors at full scale. part i: Geometry modeling and aerodynamics," *International journal for numerical methods in fluids*, vol. 65, no. 1-3, pp. 207–235, 2011.

[32] W. Malalasekera and H. Versteeg, "An introduction to computational fluid dynamics," *The finite volume method, Harlow: Prentice Hall*, p. 1995, 2007.

[33] P. Benham, R. Crawford, and C. Armstrong, "Mechanics of engineering materials, 1996," *Harlow Longman Group*.

[34] H. E. Boyer *et al.*, *Atlas of fatigue curves*. Asm International, 1985.

[35] R. L. Norton, "Machine design: an integrated approach, 2000," 2011.

[36] J. Jonkman, S. Butterfield, W. Musial, and G. Scott, "Definition of a 5-mw reference wind turbine for offshore system development," tech. rep., National Renewable Energy Lab.(NREL), Golden, CO (United States), 2009.

[37] W. S. VESTAS, "General description 4mw platform," 2017.

[38] T. Batu and H. G. Lemu, "Fatigue life study of false banana/glass fiber reinforced composite for wind turbine blade application," in *International Workshop of Advanced Manufacturing and Automation*, pp. 29–40, Springer, 2020.

[39] H. J. Sutherland, "On the fatigue analysis of wind turbines," 1999.

[40] R. C. Juvinall and K. M. Marshek, *Fundamentals of Machine Component Design*. John Wiley & Sons, 2020.

[41] J. L. Zeman, F. Rauscher, and S. Schindler, *Pressure vessel design: the direct route*. Elsevier, 2006.

[42] R. C. Rice, B. N. Leis, and D. Nelson, *Fatigue design handbook*, vol. 10. Society of Automotive Engineers, 1988.

[43] J. A. Collins, H. R. Busby, and G. H. Staab, *Mechanical design of machine elements and machines: a failure prevention perspective*. John Wiley & Sons, 2009.

[44] S. Andersen, P. Bach, W. Bonne, C. Kensche, H. Lilholt, A. Lystrup, and W. Sys, "Fatigue of materials and components for wind turbine rotor blades," 1996.